In Vivo Evaluation of Wearable Head Impact Sensors

Lyndia C. Wu,[1] Vaibhav Nangia,[2] Kevin Bui,[1] Bradley Hammoor,[1] Mehmet Kurt,[1] Fidel Hernandez,[2] Calvin Kuo,[2] and David B. Camarillo[1,2]

[1]Department of Bioengineering, Stanford University, 443 Via Ortega, Stanford, CA 94305, USA; and [2]Department of Mechanical Engineering, Stanford University, Stanford, CA, USA

Associate Editor Joel D. Stitzel oversaw the review of this article.

Abstract—Inertial sensors are commonly used to measure human head motion. Some sensors have been tested with dummy or cadaver experiments with mixed results, and methods to evaluate sensors *in vivo* are lacking. Here we present an *in vivo* method using high speed video to test teeth-mounted (mouthguard), soft tissue-mounted (skin patch), and headgear-mounted (skull cap) sensors during 6–13 g sagittal soccer head impacts. Sensor coupling to the skull was quantified by displacement from an ear-canal reference. Mouthguard displacements were within video measurement error (<1 mm), while the skin patch and skull cap displaced up to 4 and 13 mm from the ear-canal reference, respectively. We used the mouthguard, which had the least displacement from skull, as the reference to assess 6-degree-of-freedom skin patch and skull cap measurements. Linear and rotational acceleration magnitudes were over-predicted by both the skin patch (with 120% NRMS error for a_{mag}, 290% for α_{mag}) and the skull cap (320% NRMS error for a_{mag}, 500% for α_{mag}). Such over-predictions were largely due to out-of-plane motion. To model sensor error, we found that in-plane skin patch linear acceleration in the anterior–posterior direction could be modeled by an underdamped viscoelastic system. In summary, the mouthguard showed tighter skull coupling than the other sensor mounting approaches. Furthermore, the *in vivo* methods presented are valuable for investigating skull acceleration sensor technologies.

Keywords—Head impact sensors, Traumatic brain injury, Wearable sensors, Instrumented mouthguard, Instrumented skin patch, Instrumented skull cap, High speed video, Soft tissue modeling.

INTRODUCTION

Traumatic brain injury biomechanics can be studied in human subjects using wearable head impact sensors that measure skull accelerations. The availability of low-power, low-cost MEMS accelerometers and gyroscopes has spawned a flurry of head impact sensing approaches both in research and for consumer use. A helmet-mounted sensor system, the head impact telemetry system (HITS), is an example of a widely used sensing option.[6,20,21] However, factors such as helmet fit and padding type may affect sensor coupling to a human head, and in turn cause measurement errors.[2,13,14] More recently, industry and academic labs have developed alternative sensors with other form factors and mounting locations such as the teeth, ear-canal, skin, and various types of headgear. For these devices, factors including fit, adhesion, soft-tissue elasticity, and hair/scalp properties may affect sensor skull coupling and measurement accuracy.

Instrumented bite blocks have been used *in vivo* as reference sensors.[9,16] A similar approach is to instrument a mouthguard, which is practical for field use in contact sports. Instrumented mouthguards have been evaluated *in vitro* with a clamped-jaw dummy as a reference.[4] One error source was introduced when the sensor was placed in a protruding tab on the mouthguard, which exhibited a mechanical resonance. The resonance led to errors in peak acceleration measurements, but root-mean-squared (RMS) acceleration errors were still within 10%. Bartsch *et al.*[1] also demonstrated accuracy using a dummy head that does not have a lower jaw to clamp the mouthguard.

Skin patch and skull cap sensors are also used in research and are becoming commercially available. Skull coupling of either approach has not been evaluated in literature. Previous studies with skin-mounted sensors and optical markers at other locations on the body (e.g., knee joint) report artifacts due to skin dynamics.[17,19,24] Differentiation of position and orientation measurements can amplify acceleration errors from such soft tissue artifacts. Therefore, some

Address correspondence to David B. Camarillo, Department of Bioengineering, Stanford University, 443 Via Ortega, Stanford, CA 94305, USA. Electronic mail: lyndiacw@stanford.edu, dcamarillo@stanford.edu

researchers have modeled soft-tissue dynamics to correct for measurement errors.[15,26] It is likely that soft tissue or textile dynamics affects sensor performance, but the effects have not been quantified for head impacts.

Sensors are commonly evaluated through *in vitro* (anthropomorphic test device) and/or *ex vivo* (postmortem human subject) methods. Both methods have the advantage of using high fidelity reference sensors rigidly attached to the skull. *In vitro* methods test sensor accuracy without confounding factors such as soft tissue motion, and are valuable for verifying sensor hardware selection and programming. *Ex vivo* methods introduce additional biofidelic factors including skull and tissue dynamics, but the effects of postmortem changes in tissue properties are unknown, and the lack of muscle forces may also affect head dynamics. Thus *in vivo* sensor evaluation may help to account for these factors. But there is a lack of *in vivo* methods, since we can neither screw reference sensors directly to the skull, nor use dangerous impact conditions in human subject studies.

Thus our objective is to develop a non-invasive *in vivo* method to evaluate head impact sensing approaches. Using this method, we will test three types of approaches: sensors fit to hard tissue (teeth), adhered to soft tissue (skin), or mounted on headgear that fits the head. Corresponding to these sensor types, we assessed skull coupling of an instrumented mouthguard, a skin patch, and a skull cap sensor in a human subject during mild soccer head impacts. Skull coupling was quantified by tracking relative displacement of the sensor from an ear-canal reference through high speed video (Fig. 1). Since the mouthguard had the least amount of relative displacement, we used its 6-degree-of-freedom (6DOF) measurements as the

reference to compare the other two sensors. To account for sensor error from soft-tissue motion, we modeled sensor-skull dynamics using a simple viscoelastic model.

METHODS

Human Subject Experiment Setup

A 26 year-old male human subject underwent soccer head impacts with clenched teeth, at initial ball speed of 7 m/s (Fig. 1a), which is the average header speed in youth soccer, and higher than that (5.7 m/s) in adults.[23] A ball launcher (Sports Tutor, Burbank, CA) helped to simulate a kicked ball, and the ball was inflated to approximately 8–9 psi. Human subject protocols in this study have been approved by the Stanford Institutional Review Board (IRB No. 26620), and informed consent was obtained from the subject.

Instrumentation

The volunteer wore a custom-fit mouthguard,[27] a skin patch adhered to skin on the mastoid process (xPatch Gen2, X2Biosystems, Inc.), and an elastic skull cap (Reebok). The mouthguard had approximately 4 mm average thickness and 7 mm height above the gum line. Electronics were placed inside the mouth to avoid tab resonance, while video markers were fixed on a light-weight protruding tab. The volunteer's head circumference measured 60.3 cm, and wore a size large elastic skull cap. The same electronics from the mouthguard were placed on a soft cardboard in the lateral insert of the skull cap.
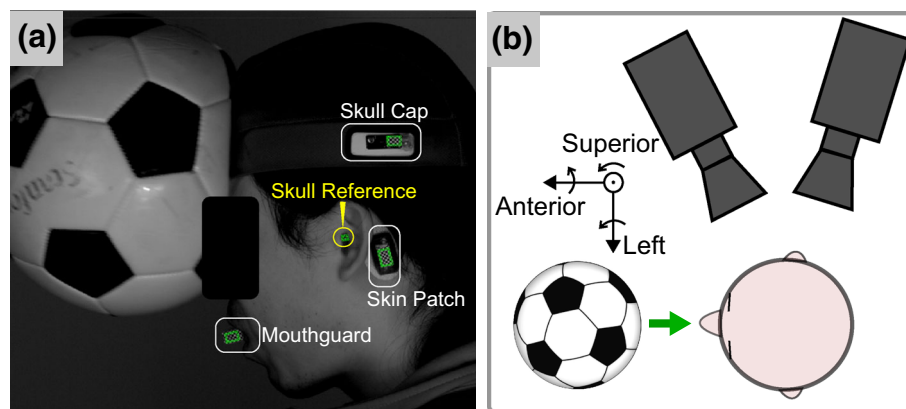

FIGURE 1. *In vivo* evaluation and comparison of instrumented mouthguard, skin patch, and skull cap. (a) A human subject underwent mild soccer head impacts, wearing all three sensors. Fiducial markers were mounted on the head, with one set on a deeply-inserted earplug (skull reference), and a set on each sensor. (b) Markers were tracked using high-speed stereo video to determine the relative motion between each sensor and the skull reference.

To enable comparison of measurements, devices were set to a low triggering threshold (4–6 g) to ensure all impacts were recorded on each device. Sensor signals were synchronized through video by aligning sensor-measured kinematics with video-derived sensor kinematics for each individual sensor. To derive sensor kinematics from video, we resolved the position and orientation of each sensor using a previously-described method of tracking fiducial markers in stereo video.[11] During synchronization, we found that skin patch motion can lag behind the mouthguard by as much as 15 ms. So we recorded 30 ms of pre-trigger data and 70 ms post-trigger.

In addition to these three sensors, the subject wore a deeply-inserted earplug as a skull reference point. Previous research confirmed skull coupling of deeply-inserted custom-fit silicone earplugs using reference sensors screwed onto the skull of a postmortem human subject.[5,22] An expandable foam earplug was inserted approximately 2 cm into the ear canal. The low mass of a foam earplug (0.2 g, compared to 5 g for a typical custom-formed silicone earplug) minimizes inertial effects and improves coupling to the ear canal.

Video Analysis of Skull Coupling

We took high speed stereo video at 1000 frames per second and 1920 × 1200 resolution (0.3 mm/pixel at distance of head), using two Phantom Miro LC320 cameras (Vision Research, Wayne, NJ), to track motion of the sensors (Fig. 1b). Fiducial markers with 1.5 mm square grids were fixed onto each sensor and the earplug to track the change in distance between grid centroids. The mouthguard, skin patch, and skull cap sensors each had 26–30 trackable points, and the earplug had 1–3 trackable points. The two cameras were positioned such that (1) the tracking grid on the deeply inserted earplug had at least 1 trackable point and (2) all three sensors were visible throughout the head impact. Due to these constraints, there was a triangulation angle of 7.4° between the cameras. Using the Camera Calibration Toolbox for Matlab,[3,10,28] we performed stereo calibration to enable 3D position tracking in the head motion space.

To verify our video method, we tracked the 4 corners of a 20 cm × 20 cm calibration grid during 6DOF motion through 4000 frames (4 s). The calibration grid moved through the same region of space as head motion, at the same distance away from the cameras as the subject. We assessed both planar and depth measurements of distance, by comparing stereo video measurements with ground truth grid distances in each frame. In addition, we derived sagittal kinematics of each sensor from video measurements, to cross validate with sensor measurements. At each time point,

positions of multiple points on the grid fixed to a sensor were used to determine the least-squares rotation matrix describing the orientation of the body-fixed frame of each sensor in the camera-fixed frame.[11] The time derivative of this rotation matrix was related to the rotational velocity of the body-fixed frame in the camera-fixed frame. We used this rotational velocity to determine linear velocity and acceleration in the moving body-fixed frame from linear position and velocity in the camera-fixed frame (Eqs. (1) and (2), where $\mathbf{v}_b$ is the linear velocity of the grid centroid in the body-fixed frame, $\mathbf{v}_c$ is the linear velocity of the grid centroid in the camera-fixed frame, ω is the rotational velocity of the grid, $\mathbf{d}_c$ is the linear position of the grid centroid in the camera-fixed frame, $\mathbf{a}_b$ is the linear acceleration of the grid centroid in the body-fixed frame, $\mathbf{a}_c$ is the linear acceleration of the grid centroid in the camera-fixed frame). Due to near-parallel arrangement of cameras, out-of-plane measurements are expected to have larger errors, and we compared 3DOF sagittal kinematics instead of full 6DOF kinematics when validating our video method.

$$\mathbf{v}_b = \mathbf{v}_c + \omega \times \mathbf{d}_c \qquad (1)$$

$$\mathbf{a}_b = \mathbf{a}_c + \omega \times \mathbf{v}_c \qquad (2)$$

Comparison of 6-DOF Sensor Kinematics

Video measurements of the ear-canal reference only allowed for 1-3 trackable points, so 6DOF kinematics could not be computed. To evaluate 6DOF measurement differences, we selected a reference device with the least relative motion to the ear-canal—the mouthguard sensor.

We transformed kinematic measurements of the skin patch and skull cap sensors to an estimated center-of-gravity (CG) location, for trials where mouthguard and skull were found to have the lowest relative displacement (see "Skull Coupling from Video" section). CG location was estimated based on a 50th percentile male human head model. First we found the projection vector from mouthguard to CG by using the upper dentition as an anatomical landmark on the model. Then we measured the projection vectors of the skin patch and skull cap sensors to the mouthguard location on our human subject through stereo video and physical measurements. We calculated the each sensor's resultant projection vectors to CG by summing its projection vector to the mouthguard and the projection vector from mouthguard to CG. Using this method, we ensure that all three devices can be transformed to the same point in space for comparison,

even though the model-estimated CG location is expected to have some error.

Linear accelerations were transformed to the CG location for comparison using the following rigid body vector relationship:

$$\mathbf{a}_{CG} = \mathbf{a}_s + \alpha \times \mathbf{r}_s + \omega \times (\omega \times \mathbf{r}_s), \quad (3)$$

where $\mathbf{a}_{CG}$ is head linear acceleration at CG, $\mathbf{a}_s$ is head linear acceleration at each sensor location, α is head angular acceleration measured by the sensor, ω is head angular velocity measured by the sensor, and $\mathbf{r}_s$ is the vector position of CG location from the sensor location.

Transformed skin patch and skull cap sensor data were compared with mouthguard reference data in the anterior–posterior (AP), left–right (LR), inferior–superior (IS) directions for linear acceleration, and the coronal, sagittal, and horizontal planes for rotational acceleration. Quantities reported include vector magnitudes and individual axis differences from all 6DOF linear acceleration, angular velocity, and angular acceleration. We performed linear regression analysis of peak kinematic values. We also reported the average deviation in peak values from the mouthguard reference, and compared the directions of head acceleration. In addition to peak values, we assessed the agreement of time traces by computing root-mean-square (RMS) difference and normalized root-mean-square (NRMS) difference for 25 samples around peak measurements.[4] To better understand the sources of sensor errors prior to transformation to CG, we also computed the RMS and NRMS differences at the sensor location. That is, we compared skin patch/skull cap signals at the skin patch/skull cap location with mouthguard reference signals projected to the skin patch/skull cap location.

Modeling of Sensor Dynamics

Model Description

Since the soccer headers were frontal hits and head motion was mainly anterior–posterior, we modeled the skin patch and skull cap translation in the anterior–posterior direction as a second order linear system with base (skull) excitation (Fig. 2a, Eq. (4)), where m_{sensor} is the combined mass of the sensor and soft tissue (kg), K_t is the effective linear spring constant of sensor-skull mounting (N/m), C_t is the effective linear damping constant of sensor-skull mounting (N s/m), d_{sensor} is the absolute displacement of the sensor (m), d_{skull} is the absolute displacement of the skull (m)

$$m_{\text{sensor}}\ddot{d}_{\text{sensor}} = -K_t(d_{\text{sensor}} - d_{\text{skull}}) - C_t(\dot{d}_{\text{sensor}} - \dot{d}_{\text{skull}})$$
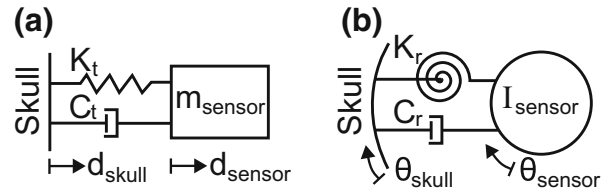$$(4)$$

(a)   **(b)**

FIGURE 2. Dynamic model description. (a) For anterior–posterior translation, we modeled each sensor-skull system as a second order linear system with a spring and a damper in parallel. These elements represent dynamics of the underlying tissue as well as the packaging and attachment of the sensors. (b) For the case of sagittal rotation, the elements are torsional springs and dampers.

We also modeled sagittal rotation of the head using a similar second order linear system (Fig. 2b, Eq. (5)).

$$I_{\text{sensor}}\ddot{\theta}_{\text{sensor}} = -K_r(\theta_{\text{sensor}} - \theta_{\text{skull}}) - C_r(\dot{\theta}_{\text{sensor}} - \dot{\theta}_{\text{skull}})$$
$$(5)$$

Model Evaluation

We used sensor data from soccer impacts to find the input-output relationship defining the skull-tissue-sensor system. Only trials where mouthguard-skull coupling was best (<0.5 mm) were modeled. We fit model parameters using mouthguard measurements as skull input, and skin patch/skull cap measurements as sensor output.

Sensor modeling was done by fitting spring, damper, and mass parameters to the input skull kinematics and output sensor kinematics. The spring-damper system takes mouthguard-measured skull motion (obtained by transforming the mouthguard kinematic signal to the sensor location) as an input and runs a forward dynamics simulation using the Matlab ode45 integrator to solve for the resulting sensor kinematics. The initial state for the system is set such that there is no relative motion between the skull and sensor and the spring is at its rest length. We used the Matlab function fmincon to find a set of spring stiffness, damping coefficient, and mass parameters that minimize the RMS error between the output model sensor kinematics and the measured sensor kinematics. The search space for these parameters are bounded to constrain the system to realistic values and the initial guess is set as the midway point between bounds. Considering that the sensors moved along with packaging and underlying soft tissue, a loose mass bound of 1–50 g was placed on the optimization to determine the mass of the system. Each impact is separately fitted in order to account for variability in impact conditions (location and force). The NRMS of the fit was used to assess the model.

In order to check the validity of the linearity assumption in our model, we examined the input-output relationship in the frequency domain by plotting the experimental and theoretical frequency response functions (FRFs). Experimental FRFs were calculated by taking the ratios of the Fast Fourier Transform (FFT) amplitudes of the skull input and skin patch output. Furthermore, the analytical frequency response of the base-excitation model depicted in Fig. 2a was compared against the experimental FRFs.

RESULTS

Skull Coupling from Video

We verified stereo video tracking to have <1 mm error in the sagittal plane (Fig. 3a). When the calibration grid was displaced or rotated in a plane per-

pendicular to the camera axis (sagittal), stereo triangulation estimated distances between points on the calibration grid with <1 mm error. When depth measurement was involved, such as during out-of-plane rotation (i.e., grid was tilted from camera plane), errors were slightly larger but still within 2 mm. Overall, more than 90% of the errors were within 0.5 mm. As an additional verification step of the video method, we compared video-derived sagittal kinematics of each sensor with those measured by the accelerometer and gyroscope in each sensor. These kinematics matched with <30% NRMS difference, even for linear acceleration double-differentiated from position tracking (Fig. 3c; Table 1).

For the mouthguard, all head impact trials ($n = 16$) showed relative displacements from the earplug of <1 mm (Fig. 4, $\mu = 0.5$ mm, $\sigma = 0.2$ mm), within video measurement error. In addition, 10 of the 16
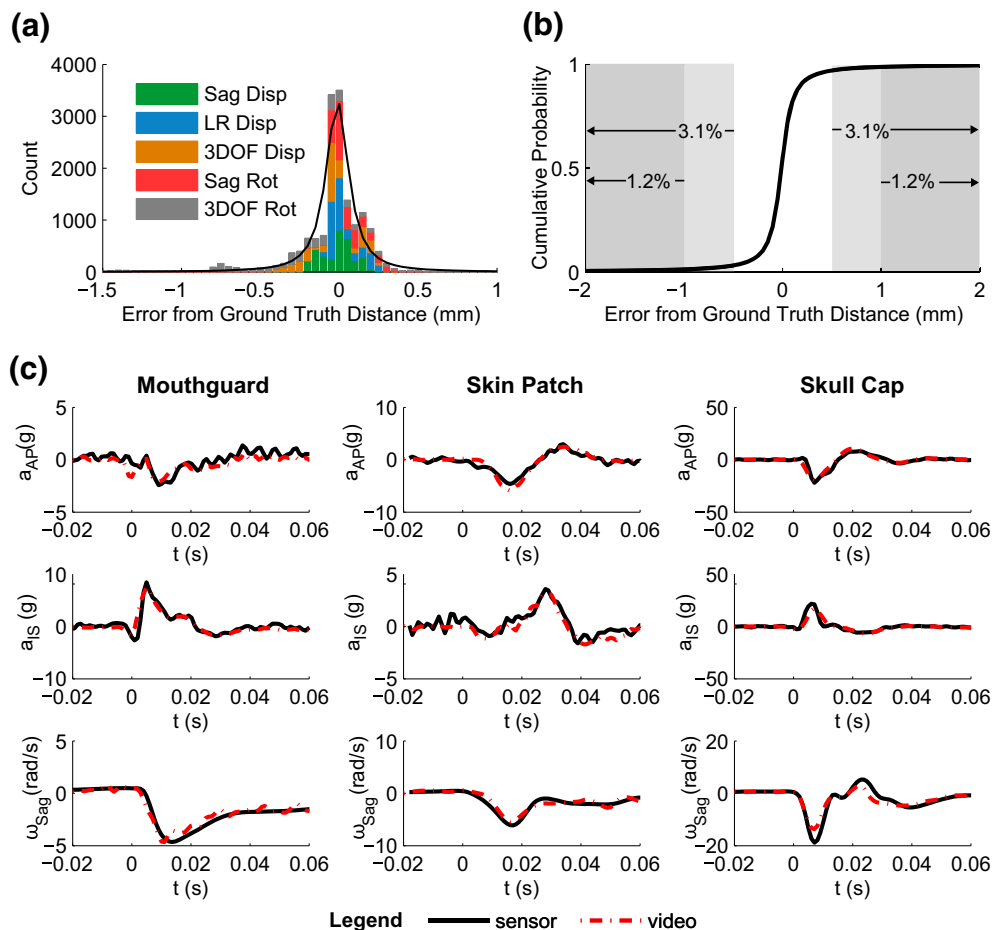

FIGURE 3. Video validation. (a) We calculated errors from video tracking using a 20 cm x 20 cm calibration grid moving through the head motion region of space. When the calibration grid displaced or rotated with a sagittal orientation (i.e., planar measurements), errors were always sub-millimeter. When depth measurement was involved, with the grid rotating in non-sagittal directions, errors were larger but still within 2 mm. (b) We fit a t location-scale distribution to the error, and there is less than 2.5% total probability of errors greater than 1 mm. (c) We also verified that video-derived sagittal kinematics agree well with those measured by the sensors, which further confirms our video measurements.

TABLE 1. RMS errors of video-tracked sagittal kinematics with respect to sensor measurements.

Device	AP linear acceleration		IS linear acceleration		Sagittal angular velocity	
	RMS (g)	NRMS (%)	RMS (g)	NRMS (%)	RMS (rad/s)	NRMS (%)
Mouthguard	1.0 (0.6)	15.5 (6)	1.8 (1)	18.1 (10)	0.6 (0.3)	12.2 (7)
Skin patch	1.4 (0.3)	13.7 (2)	1.3 (1)	29.3 (30)	2.1 (0.7)	28.6 (9)
Skull cap	4.4 (3)	16.0 (9)	2.1 (1)	12.5 (5)	2.0 (2)	13.2 (11)

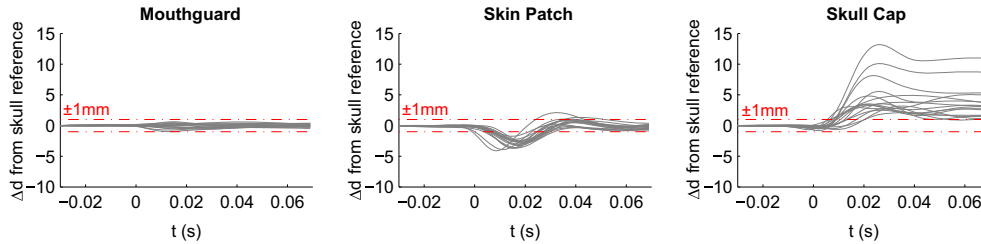Average RMS and NRMS errors are reported with standard deviation in parentheses.

FIGURE 4. Sensor coupling evaluation. Using high speed video, we compared the relative displacements of the three sensors from the skull. Among 16 trials, the mouthguard always had sub-millimeter displacements from the skull within video error, while the other two sensors had higher displacements.

trials showed relative mouthguard displacements of within 0.5 mm. In contrast, the skin patch sensor displaced by 2–4 mm ($\mu = 3$ mm, $\sigma = 0.7$ mm) at the moment of head impact; the skull cap sensor displaced by 2–13 mm ($\mu = 5$ mm, $\sigma = 3$ mm).

6-DOF Sensor Kinematics

Using the mouthguard as a reference, head acceleration peak magnitudes for the 10 trials averaged 9.3 ± 2 g in linear acceleration and 750 ± 300 rad/s^2 in rotational acceleration. Skin patch estimation of head linear and angular acceleration peak values were over-predicted by 15 ± 7 g and 2500 ± 1200 rad/s^2 on average, respectively; the skull cap values were over-predicted by 50 ± 31 g and 4300 ± 2700 rad/s^2 (Table 2). These over-predictions were the average differences in peaks between the sensor measurements and the reference (mouthguard) measurements. Figure 5a also shows the over-predictions in peak magnitudes, with patch/cap predictions scattered above and away from the $m = 1$ reference line. In addition, patch and cap peak vector magnitudes and all individual component peaks had large variances, and did not correlate well with the mouthguard reference (Supplemental Fig. S1). When y-intercept is forced to be 0 in linear regression analysis, the coefficient of determination is sometimes negative (Supplemental Table S1), indicating that the residual error in the fit is greater than the variance in the data. To evaluate dynamic relationships among sensors, Table 2 reports the time lag/lead between the mouthguard peak value and patch/cap

peak values. The skin patch linear acceleration magnitude peak was the most consistent, occurring 13 ± 2 ms after the mouthguard peak.

The skin patch and skull cap also predicted different directions of head motion compared with the mouthguard. Figure 5b and Table 2 show the differences in kinematic vectors at the moment of peak magnitude. The mouthguard reference measured head motion to exhibit mostly planar motion with anterior–posterior (AP) linear acceleration and sagittal rotation. In contrast, skin patch motion was mostly out-of-plane with left translation and horizontal rotation, and the skull cap was not in a consistent direction. Breaking magnitudes down into per-component comparisons, Fig. 6 shows sample 6DOF kinematic waveforms of a representative impact with mostly anterior–posterior motion. We observe over-predictions of kinematics in all axes, including out-of-plane (non-sagittal) directions. In fact, the highest peaks for the skin patch all occur in out-of-plane axes: left–right (LR) linear acceleration and horizontal rotation. The skin patch signals also show damped oscillatory behavior. Table 3 shows RMS and NRMS errors of the skin patch and skull cap in 6DOF. All magnitude errors were above 100%. At sensor location, the linear acceleration RMS and NRMS errors were lower than those at the CG (comparing Table 3 and Supplemental Table S2). At sensor, linear acceleration magnitude had 18% NRMS error for the skin patch, and 60% NRMS error for the skull cap, compared to 120% and 320% when projected to CG. Angular velocity and angular accelera-
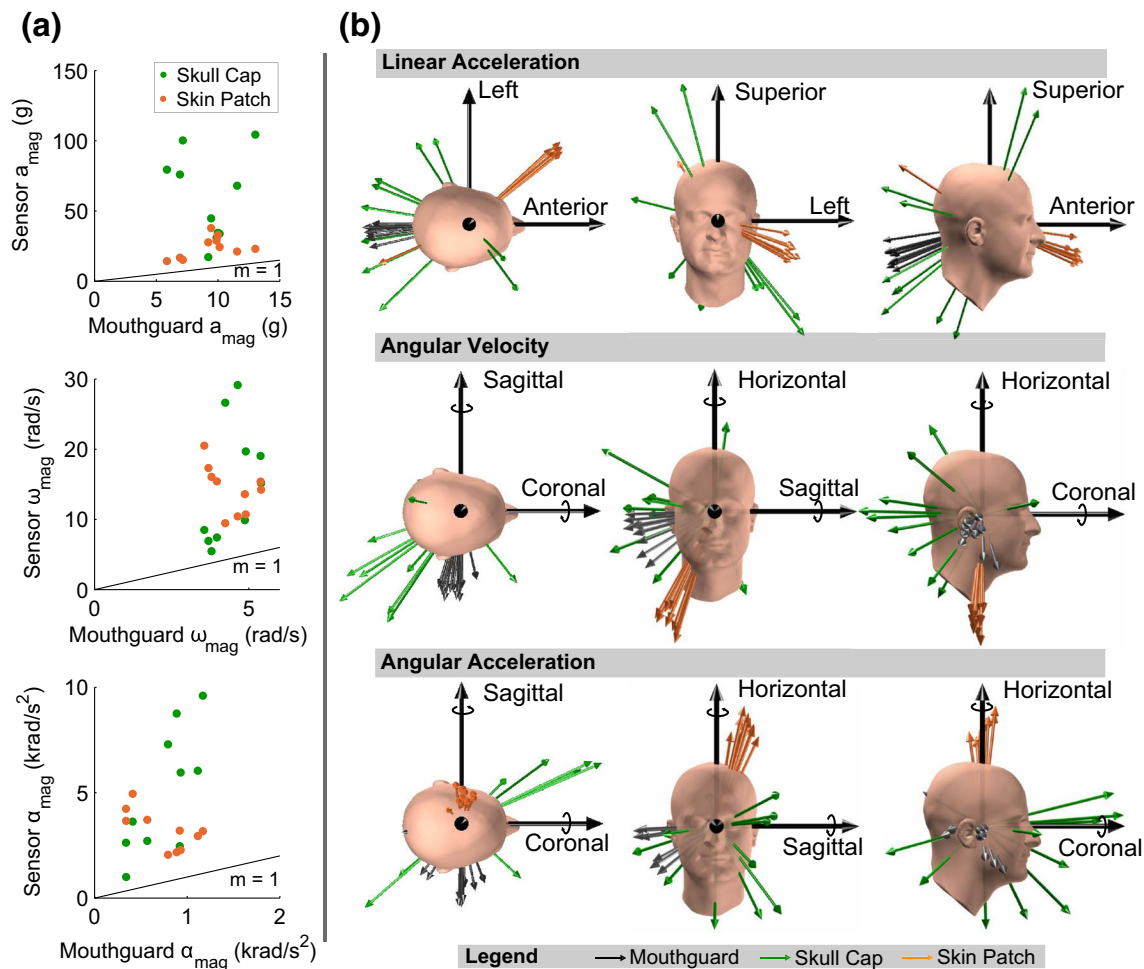
FIGURE 5. Comparing magnitude and direction of peak kinematics at head CG. Skin patch and skull cap measurements were compared with the mouthguard, which was used as the skull reference. (a) shows scatter plots of peak magnitudes of linear acceleration, angular velocity, and angular acceleration. The $m = 1$ reference line represents the ideal correlation when skin patch and skull cap match the reference. In (b), we plot vectors showing the direction of head accelerations and velocities at the moment of peak magnitude (lengths of vectors are not to scale). The mouthguard, or skull reference, measured head motion to exhibit mainly posterior or superior linear acceleration, with sagittal rotation. The other two sensors, however, predict different directions of acceleration/velocity.

tion were independent of the location on the head, and had the same high errors at both sensor location and CG (skin patch: 290%, skull cap: 500%).

Sensor Modeling

Identified model parameters are detailed in Table 4, including the NRMS errors of the fit. The statistics are generated from: all trials for skin patch AP translation; 7 of 10 trials for skin patch sagittal rotation; and 8 of 10 trials for cap AP translation. Since this is a very simplified 2-element model, we did not expect all trials to fit to the model. In order to report meaningful parameter estimates, we omitted trials where the model could not fit to the data. Some trials were omitted for patch sagittal rotation since the input mouthguard signal lagged behind the patch measurement. In such cases, the mouthguard signal could not be used as input for modeling. Instead, the input to the system likely came from other coupled axes. Some trials were omitted for skull cap AP translation, since reasonable estimates of model parameters could not be found due to sharp spikes in the signal, which likely resulted from direct soccer ball impact. For all trials of skull cap sagittal rotation, the mouthguard signal consistently lagged behind the skull cap signal, and the model failed to fit. Figure 7 shows sample traces comparing the model fit and measured signals. Overall, model fits were the most consistent for skin patch in AP translation. The average estimated mass of the skin patch system (8.5 g) is greater than mass of the sensor itself (5 g), showing that some underlying tissue mass was also activated during the impacts.

TABLE 2. Comparing skin patch and skull cap kinematic peak values with mouthguard reference at head CG.

Device	Avg peak Diff (g)	Std peak diff (g)	Avg peak Delay (ms)	Std peak Delay (ms)	Avg direction Diff (θ)	Std direction Diff (θ)
Linear acceleration magnitude						
Skin patch	+15	±7	+13	±2	123	±26
Skull cap	+50	±31	+4	±4	54	±38

Device	Avg peak Diff (rad/s)	Std peak diff (rad/s)	Avg peak Delay (ms)	Std peak Delay (ms)	Avg direction Diff (θ)	Std direction Diff (θ)
Angular velocity magnitude						
Skin patch	+9.9	±4	−7	±15	51	±11
Skull cap	+10.3	±8	−9	±12	58	±22

Device	Avg peak Diff (rad/s^2)	Std peak diff (rad/s^2)	Avg peak Delay (ms)	Std peak Delay (ms)	Avg direction Diff (θ)	Std direction Diff (θ)
Angular acceleration magnitude						
Skin patch	+2500	±1200	+15	±9	116	±22
Skull cap	+4300	±2700	+4	±3	98	±27

Positive (+) sign indicates over-prediction for average peak difference, and indicates delay for average peak delay.
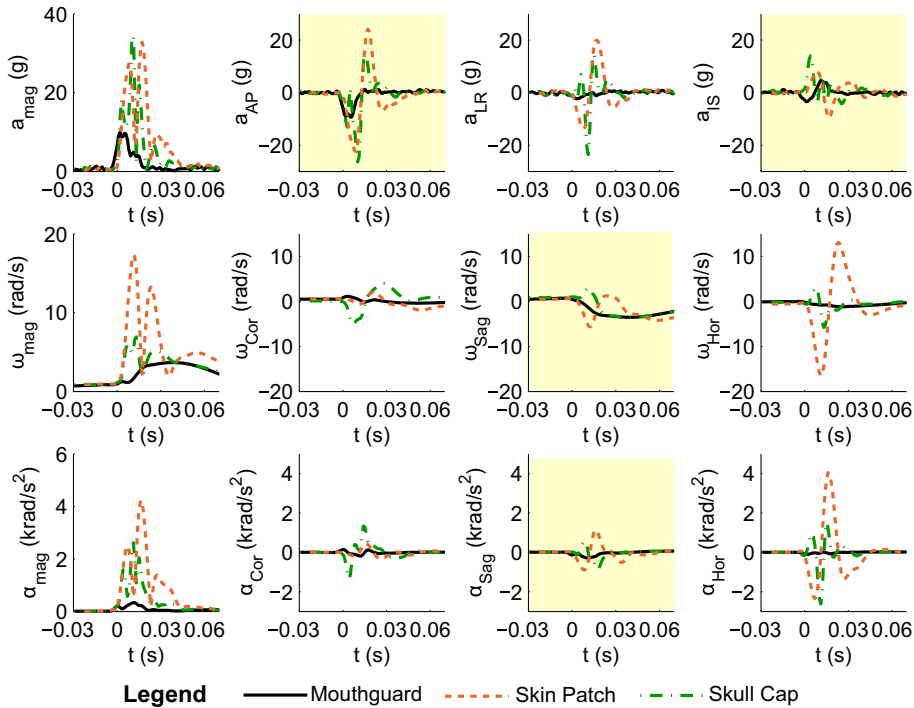

FIGURE 6. Comparing 6DOF kinematics at head CG in a sample impact. Measurements from skin patch and skull cap are compared with the mouthguard reference. Both sensors over-predict accelerations in the sagittal plane (highlighted axes) as well as out-of-plane axes.

For skin patch AP translation, where the model could be fit to all 10 trials with relatively low variance in model parameters, we verified the linear system assumption and examined the frequency response around the resonant frequency of the model. Figures 8a and 8b show the FFT amplitudes for the

mouthguard (skull) input and skin patch (sensor) output, respectively. The FRFs, which are the ratio of output FFT amplitude to the input FFT amplitude, are shown for all trials in Fig. 8c. We compared these with a theoretical FRF (red line), which is the frequency response of the transfer function for the

TABLE 3. Sensor RMS differences with respect to mouthguard time traces at head CG.

Device	Parameter	Linear acceleration		Angular velocity		Angular acceleration	
		RMS (g)	NRMS (%)	RMS (rad/s)	NRMS (%)	RMS (rad/s^2)	NRMS (%)
Skin patch	AP translation/coronal Rotation	12.5 (4)	120 (30)	1.2 (0.6)	78 (29)	182 (114)	44 (27)
	LR translation/sagittal Rotation	8.8 (3.3)	300 (160)	2.2 (0.6)	48 (16)	786 (170)	120 (62)
	IS translation/horizontal rotation	5.1 (1.6)	70 (30)	7.5 (2.2)	700 (380)	1772 (516)	860 (500)
	Magnitude	10.8 (4.5)	120 (40)	5.7 (1.9)	150 (76)	1539 (552)	290 (230)
Skull cap	AP translation/coronal rotation	12.4 (6.8)	140 (110)	4.8 (2.5)	370 (280)	1858 (1290)	460 (340)
	LR translation/sagittal rotation	15.7 (8.3)	510 (300)	4 (2.5)	83 (52)	1349 (823)	160 (60)
	IS translation/horizontal rotation	19 (13.2)	250 (180)	2.6 (1.5)	330 (450)	945 (565)	590 (660)
	Magnitude	25.6 (16.1)	320 (260)	4.6 (3.5)	110 (80)	2233 (1379)	500 (140)

Note: average RMS and NRMS errors are reported with standard deviation in parentheses.

TABLE 4. Model parameters.

Device	K_t (N/m)	C_t (N-s/m)	m_{sensor} (g)	f (Hz)	ζ	NRMS (%)
AP translation						
Skin patch	189.4 (46)	0.67 (0.16)	8.5 (1.6)	23.8 (2.3)	0.27 (0.09)	20.4 (11)
Skull cap	396 (125)	1.43 (0.40)	12.4 (9.6)	35.2 (16)	0.40 (0.17)	31.1 (11)

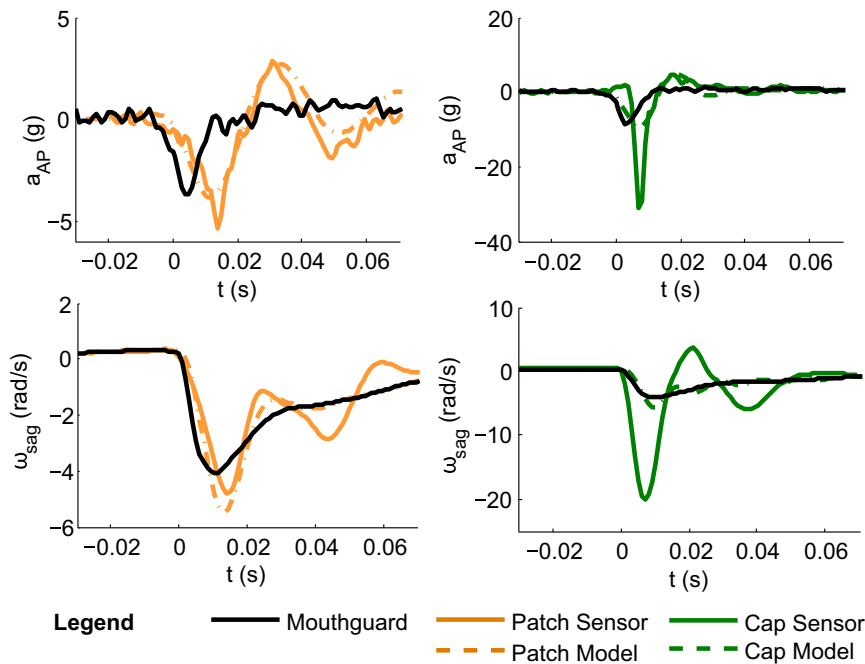| Device	K_r (N m/rad)	C_r (N m/rad s)	I_{sensor} (kg m^2)	f (Hz)	ζ	NRMS (%)
Sagittal rotation						
Skin patch	0.30 (0.08)	4×10 (1×10^{-4})	4.5×10 (1×10^{-6})	41.6 (5)	0.20 (0.08)	20.0 (8)
Skull cap	–	–	–	–	–	–

FIGURE 7. Model predictions for skin patch and skull cap. For skin patch AP translation, sagittal rotation, and skull cap AP translation, we could fit underdamped second order linear systems to model sensor output. For skull cap *y* rotation, the mouthguard (skull) input lagged behind the sensor output, and thus this axis could not be modeled using this simple model.

model in Fig. 2 with the average model parameters (Table 4). As shown, 9 of the 10 trials had FRFs with amplitudes and peak frequencies within a ±1 stan- dard deviation confidence interval, which validates the linearity assumption, since a linear system exhibits a consistent FRF.[7]
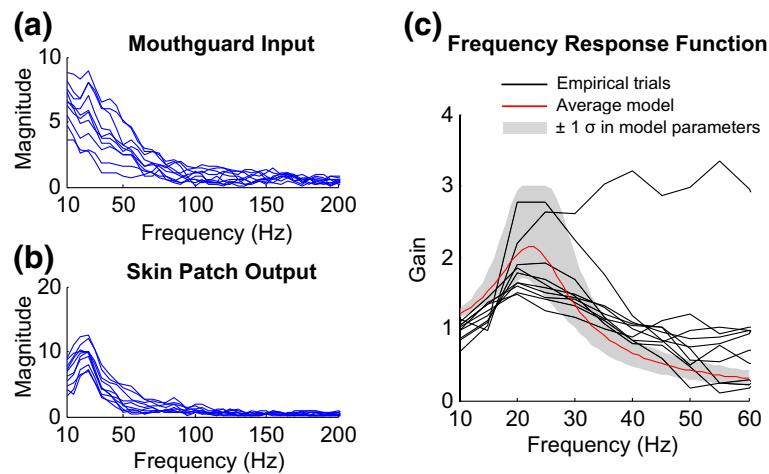
FIGURE 8. Frequency response function of skin patch in AP linear acceleration. The FFT of the mouthguard input (a) and skin patch output (b) both show peak amplitudes occurring in a low frequency range. The frequency response function of the system (c) shows that for 9 of 10 of the trials modeled, the frequency response functions are similar, within 1 standard deviation (shaded region) of the theoretical model (red line), which further demonstrates linearity of the system.

DISCUSSION

In this study, we developed an *in vivo* method to quantify skull coupling of teeth-mounted (mouthguard), soft tissue-mounted (skin patch), and headgear-mounted (skull cap) sensors. All mouthguard-skull displacements were within video measurement error. This was an expected outcome for mild impacts with clenched teeth, since the mouthguard is custom-formed to the teeth. It does confirm that *in vivo* clenching force can hold the mouthguard in place for the soccer impact conditions tested. On the field, other practical factors such as mandible motion and variations in mouthguard fabrication may affect performance. Unanticipated impacts with open jaw may also pose a problem for the mouthguard. Thus field mouthguard coupling remains to be tested. However, in anticipated impacts, the teeth are likely clenched, resulting in similar conditions as our tested scenario.

Non-rigid skull coupling led to skull measurement errors in skin patch and skull cap sensors. Both sensor showed over-predictions of peak head CG kinematics. Such over-predictions resulted from measurements of significant out-of-plane motion, while head motion was mostly sagittal. In fact, the skin patch and skull cap often measured acceleration peaks in a different vector direction from the mouthguard reference with >50° deviation (Table 2). With the over-predictions and differences in direction, raw data from these sensors likely cannot be directly used to predict or study injury risks. For example, we looked at the differences in injury risk prediction for the mild soccer impact based on government standard criteria, including a translational criterion, head injury criterion (HIC[8]), and a rotational criterion, brain injury criterion

(BrIC[25]). The skull cap linear acceleration signals yield HIC values of greater than 250, which has been cited as the concussion threshold,[18] for 4 of the 10 trials. Both skin patch and skull cap angular velocities predict BrIC values up to around 0.4, which is more than 20% risk of Abbreviated Injury Scale (AIS) 2+ injury.[25] On the other hand, the mouthguard signals predict low HIC values of 1.3 ± 0.6 and BrIC values of 0.015 ± 0.008. Thus sensor errors need to be corrected *via* models, and/or reduced by improving skull coupling.

In the primary plane of motion (sagittal), a simple viscoelastic model approximated single-degree-of-freedom skin-sensor dynamics, in agreement with previous studies of lower-limb soft tissue dynamics.[15,26] As a feature of a linear dynamic system, the time lag between skin patch translation and skull translation was consistently around 13ms (Table 2), due to viscoelasticity of the skull-skin-sensor system. Skin patch motion in this axis had linear model fits with low variance in parameters (Table 4). From the frequency response of the system (Fig. 8), we further confirm the underlying linear dynamics of the system. For the soccer impact, the skull input excited a frequency range that includes the resonant frequency of the skull-skin-sensor system (20–30 Hz), where the gain of the system is maximum. However, if the head is driven at a different input frequency (i.e., a different input duration) and/or at considerably higher amplitudes, the peak gain may vary, or a different mode of the system may be excited. Therefore, it would be an oversimplification to use a static gain term to estimate head acceleration.

Behavior of the skull cap sensor, especially in rotation, was less predictable than the skin patch sensor, varying from impact to impact. The time lag

between cap and skull motion had large variance (Table 4), indicating inconsistent behavior. This is likely due to direct impact of the skull cap by the ball. Ball force and impact location were important factors for the skull cap system not accounted for by the simple linear model. During our experiments, the skull cap sometimes completely dislocated from the head (results not included since skull cap was not in camera view). However, it is possible that for other impact conditions, such as helmeted impacts, the skull cap may have less relative motion from the skull.

Although the modeling method shows promise in simulating soft tissue behavior, this may not be sufficient to correct for sensor error. Skin patch linear acceleration in the anterior–posterior direction had the lowest variance in the optimized model parameters. To estimate skull input from skin patch measurements, an inverse dynamics simulation can be performed using average model parameters. However, a single mass-spring-damper model would only help to mitigate skin patch errors in 1DOF, and the variability in tissue response across different impact conditions and subjects can pose a challenge in developing a universal model. Also, referring to Supplemental Table S2, we show that the linear acceleration errors at head CG are much higher than those at the sensor locations. This indicates amplification of rotational velocity and acceleration errors when measurements are projected to CG. Therefore, better models or design changes to mitigate rotational errors may help significantly improve sensor performance.

The *in vivo* methods in this study have some limitations. First, only mild impacts were assessed in a single human subject. We tested low-speed 7 m/s impacts for protection of the human subject, while field ball speeds could reach up to 17 m/s.[23] With only one subject and one impact condition, the outcomes are likely subject to variability in soft tissue properties, skull cap fit, mouthguard fit, and impact location/severity. The head acceleration levels (6–13 g) were also low compared with injury-level accelerations on the field,[12] for protection of human subjects. Second, high speed stereo video tracking was limited by the need to deeply insert the ear-canal reference for tight skull coupling. This led to near-parallel arrangement of cameras and a low number of trackable ear-canal points. As a result, we could not derive 6DOF reference measurements from the skull reference. Third, we made the assumption that the ear canal skull reference is rigidly attached to the skull. This limitation is difficult to eliminate in an *in vivo* study. However, the fact that the mouthguard and the ear reference showed low relative motion gives confidence by cross validating these two mounting locations approximately 10 cm apart on the head. Fourth, mouthguard bite force was not controlled or measured in the experiment. At the low acceleration levels in this experiment, we do not expect bite force to significantly change results. However, at higher accelerations, bite force may need to be quantified. Lastly, in practice, higher degree-of-freedom dynamic models with more elements/parameters may be necessary to predict both in-plane and out-of-plane sensor errors.

In summary, we have developed a method to quantify skull coupling of wearable head impact sensors *in vivo*, and evaluated some common sensing approaches. The instrumented mouthguard was shown to have close skull coupling when clenched during mild soccer head impacts. The skin patch and skull cap devices had higher displacements from the skull. Raw data from sensors without close skull coupling should be interpreted cautiously both in trauma research and clinical assessment. To mitigate insufficient coupling, design modifications and modeling may help to reconstruct skull motion.

ELECTRONIC SUPPLEMENTARY MATERIAL

The online version of this article (doi: 10.1007/s10439-015-1423-3) contains supplementary material, which is available to authorized users.

CONFLICT OF INTEREST

The authors have no personal or financial conflicts of interest related to this study.

REFERENCES

[1]Bartsch, A., S. Samorezov, E. Benzel, V. Miele, and D. Brett. Validation of an ''intelligent mouthguard'' single event head impact dosimeter. *Stapp Car Crash J.* 58:1–27, 2014.
[2]Beckwith, J. G., R. M. Greenwald, and J. J. Chu. Measuring head kinematics in football: correlation between the head impact telemetry system and hybrid III headform. *Ann. Biomed. Eng.* 40(1):237–248, 2012.
[3]Bouguet, J. Y. Camera Calibration Toolbox for Matlab. http://www.vision.caltech.edu/bouguetj/calib_doc/, 2013.

[4]Camarillo, D. B, P. B. Shull, J. Mattson, R. Shultz, and D. Garza. An instrumented mouthguard for measuring linear and angular head impact kinematics in American football. *Ann. Biomed. Eng.* 41 (9): 1939–1949, 2013. .

[5]Christopher, J. J., M. R. Sochor, J. Pellettiere, and R. S. Salzar. Assessment of Ear- and Tooth-Mounted Accelerometers as Representative of Human Head Response. *SAE Technical Paper No. 2013-01-0805*, 2013.

[6]Duma, S. M., S. J. Manoogian, W. R. Bussone, P. G. Brolinson, M. W. Goforth, J. J. Donnenwerth, R. M. Greenwald, J. J. Chu, and J. J. Crisco. Analysis of real-time head accelerations in collegiate football players. *Clin. J. Sport Med.* 15(1):3–8, 2005.

[7]Ewins, D. J. *Modal Testing: Theory, Practice and Application,* 2nd edn. Hertfordshire: Research Studies Press Ltd., 2000.

[8]Federal Motor Vehicle Safety Standards (FMVSS). 571.202a. Section 571, Standard 202a-Head restraints, 2014. .

[9]Funk, J. R., J. M. Cormier, C. E. Bain, H. Guzman, and E. Bonugli. Validation and Application of a Methodology to Calculate Head Accelerations and Neck Loading in Soccer Ball Impacts. *SAE Technical Paper No. 2009-01-0251*, 2009.

[10]Heikkila, J. and O. Silvén. A Four-step Camera Calibration Procedure with Implicit Image Correction. In: Proceedings of IEEE Computer Society Conference on Computer Vision and Pattern Recognition, 1997, pp. 1106–1112.

[11]Hernandez, F., P. B. Shull, and D. B. Camarillo. Evaluation of a laboratory model of human head impact biomechanics. *J. Biomech.*, 2015 (in press).

[12]Hernandez, F., L. C. Wu, M. C. Yip, K. Laksari, A. R. Hoffman, J. R. Lopez, G. A. Grant, S. Kleiven, and D. B. Camarillo. Six degree-of-freedom measurements of human mild traumatic brain injury. *Ann. Biomed. Eng.* 43(8):1918–1934, 2014.

[13]Higgins, M., P. D. Halstead, L. Snyder-Mackler, and D. Barlow. Measurement of impact acceleration: mouthpiece accelerometer versus helmet accelerometer. *J. Athl. Train.* 42(1):5–10, 2007.

[14]Jadischke, R., D. C. Viano, N. Dau, A. I. King, and J. McCarthy. On the accuracy of the Head Impact Telemetry (HIT) System used in football helmets. *J. Biomech.* 46(13):2310–2315, 2013.

[15]Kim, W., A. S. Voloshin, S. H. Johnson, and A. Simkin. Measurement of the impulsive bone motion by skin-mounted accelerometers. *J. Biomech. Eng.* 115(1):47–52, 1993.

[16]Knox, T. Validation of Earplug Accelerometers as a Means of Measuring Head Motion. *SAE Technical Paper No. 2004-01-3538*, 2004.

[17]Lucchetti, L., A. Cappozzo, A. Cappello, and U. D. Croce. Skin movement artefact assessment and compensation in the estimation of knee-joint kinematics. J. Biomech. 31(11):977–984, 1998.

[18]Pellman, E. J., D. C. Viano, A. M. Tucker, and I. R. Casson. Concussion in professional football, part 1: reconstruction of game impacts and injuries. *Neurosurgery* 53(4):796, 2003.

[19]Reinschmidt, C., B. M. Nigg, A. Lundberg, A. J. van den Bogert, and N. Murphy. Effect of skin movement on the analysis of skeletal knee joint motion during running. *J. Biomech.* 30(1):729–732, 1997.

[20]Rowson, S. and S. M. Duma. Development of the STAR evaluation system for football helmets: integrating player head impact exposure and risk of concussion. *Ann. Biomed. Eng.* 39(8): 2130–2140, 2011.

[21]Rowson, S., J. G. Beckwith, J. J. Chu, D. S. Leonard, R. M. Greenwald, and S. M. Duma. A six degree of freedom head acceleration measurement device for use in football. *J. Appl. Biomech.* 27(1):8–14, 2011.

[22]Salzar, R. S., C. R. Dale Bass, and J. A. Pellettiere. Improving earpiece accelerometer coupling to the head. *SAE Technical Paper No. 2008-01-2978*, 2014.

[23]Shewchenko, N., C. Withnall, M. Keown, R. Gittens, and J. Dvorak. Heading in football. Part 1: development of biomechanical methods to investigate head response. *Br. J. Sports Med.* 39(Suppl 1):10–25, 2005.

[24]Shultz, R., A. E. Kedgley, and T. R. Jenkyn. Quantifying skin motion artifact error of the hindfoot and forefoot marker clusters with the optical tracking of a multi-segment foot model using single-plane fluoroscopy. *Gait Posture* 34(1):44–48, 2011.

[25]Takhounts, E. G., M. J. Craig, K. Moorhouse, J. McFadden, and V. Hasija. Development of brain injury criteria (BrIC). *Stapp Car Crash J.* 57:243–266, 2013.

[26]Trujillo, D. M. and H. R. Busby. A mathematical method for the measurement of bone motion with skin-mounted accelerometers. *J. Biomech. Eng.* 112:229–231, 1990.

[27]Wu, L. C., L. Zarnescu, V. Nangia, B. Cam, and D. B. Camarillo. A head impact detection system using SVM classification and proximity sensing in an instrumented mouthguard. *IEEE Trans. Biomed. Eng.* 61(11):2659–2668, 2014.

[28]Zhang, Z. Flexible camera calibration by viewing a plane from unknown orientations. In: Proceedings of the Seventh IEEE International Conference on Computer Vision, vol. 1, pp. 666–673. 1999.